

26 .
27 .
28 .

Contents

1	1 Introduction	2
2	2 Data Set and Monte Carlo Samples	3
3	3 Event Selection	5
3.1	Tracking, PID, $\pi^0/\eta^{(\prime)}$ and K_S^0 Reconstruction	5
3.2	Single Tag Selection	6
3.3	Background Analysis	8
4	4 Model Independent Partial Wave Analysis	11
4.1	Signal Candidate Selection	11
4.2	Background Analysis	11
4.3	MIPWA method	14
4.4	S-wave parameterization at the K^+K^- threshold	16
5	5 Amplitude Analysis	18
5.1	Fit Method	18
5.2	Fit Fraction	19
5.3	Fit Result	20
5.4	Sytematic Uncertainties	21
6	6 Branching Fraction Measurements	26
6.1	Results of Branching Fraction	26
6.2	Systematic Uncertainties	26
7	7 Summary	29
Appendices		31
A	A Subtract of the Secondary proton	32

1 Introduction

The decay $D_s^+ \rightarrow K^+ K^- \pi^+$ is a Cabibbo-favored (CF) channel and has a large branching fraction for the D_s meson. Thus, this decay channel is usually used to normalize measurements of decay chains involving charm quarks.

Knowledge of the decay amplitude allows us to properly account for interference effects when measuring absolute hadronic branching fractions of D_s mesons.

Below is the table of previous analyses of this decay channel.

Decay mode	<i>BABAR</i>	Decay fraction (%)	
		E687	CLEO-c
$\bar{K}^*(892)^0 K^+$	$47.9 \pm 0.5 \pm 0.5$	$47.8 \pm 4.6 \pm 4.0$	$47.4 \pm 1.5 \pm 0.4$
$\phi(1020) \pi^+$	$41.4 \pm 0.8 \pm 0.5$	$39.6 \pm 3.3 \pm 4.7$	$42.2 \pm 1.6 \pm 0.3$
$f_0(980) \pi^+$	$16.4 \pm 0.7 \pm 2.0$	$11.0 \pm 3.5 \pm 2.6$	$28.2 \pm 1.9 \pm 1.8$
$\bar{K}_0^*(1430)^0 K^+$	$2.4 \pm 0.3 \pm 1.0$	$9.3 \pm 3.2 \pm 3.2$	$3.9 \pm 0.5 \pm 0.5$
$f_0(1710) \pi^+$	$1.1 \pm 0.1 \pm 0.1$	$3.4 \pm 2.3 \pm 3.5$	$3.4 \pm 0.5 \pm 0.3$
$f_0(1370) \pi^+$	$1.1 \pm 0.1 \pm 0.2$...	$4.3 \pm 0.6 \pm 0.5$
Sum	$110.2 \pm 0.6 \pm 2.0$	111.1	$129.5 \pm 4.4 \pm 2.0$
χ^2/NDF	$\frac{2843}{(2305-14)} = 1.2$	$\frac{50.2}{33} = 1.5$	$\frac{178}{117} = 1.5$
Events	96307 ± 369	701 ± 36	12226 ± 22

Figure 1: previous analyses

From figure.1 [1], we can see an obvious difference of decay fraction of $f_0(980) \pi^+$ between BARBAR and CLEO-c. E687 used about 700 events and the E687 model did not take $f_0(1370) \pi^+$ into account. For CLEO-c, about 14400 events with purity about 84.9% were selected with single tag method. The analysis of BARBAR used about 100000 events with purity about 95%. In this analysis with double tag method, we can get a nearly background free data sample, that will be good to perform the amplitude analysis.

2 Data Set and Monte Carlo Samples

We use 3.195 fb^{-1} data set collected at $E_{cm} = 4.178\text{ GeV}$ by BESIII detector in 2016. Both data sample and Monte Carlo samples are reconstructed under BOSS7.0.3. Totally 35 rounds of generic MC with each round equaling to data size are used for background study. They are available at `/besfs3/offline/data/703-1/4180/mc/`.

For the Signal MC, we generate the signal events with one D_s decaying to signal mode using the generator “DIY”, in which the parameters are obtained from the fit to data. PHSP MC and Signal MC are used in MC integration required for the amplitude fit. The Signal MC is also used in the input/output check.

Table 1: Component and corresponding size, assume luminosity = 3195/pb.

Component	cross section (pb)	Size(M)	directory
$D^0 D^0$	179	0.5719	D0D0
$D^+ D^-$	197	0.6294	DpDm
$D^{*0} D^0$	1211	3.8691	DST0D0
$D^{*+} D^-$	1296	4.1407	DSTpDm
$D^{*0} D^{*0}$	2173	6.9427	DST0DST0
$D^{*+} D^{*-}$	2145	6.8533	DSTpDSTm
$D_s^+ D_s^-$	7	0.0225	DsDs
$D_s^{*+} D_s^-$	961	3.0700	DsSTDs
$DD^* \pi^+$	383	1.2237	DDSTPIp
$DD^* \pi^0$	192	0.6134	DDSTPI0
$DD \pi^+$	50	0.1598	DDPIp
$DD \pi^0$	25	0.0799	DDPI0
Component	cross section (nb)	Size(M)	
$q\bar{q}$	13.8	44.0910	qq
$\gamma J/\psi$	0.40	1.2780	RR1S
$\gamma \psi(2S)$	0.42	1.3419	RR2S
$\gamma \psi(3770)$	0.06	0.1917	RR3770
$\tau\tau$	3.45	11.0228	tt
$\mu\mu$	5.24	16.7418	mm
ee	423.99	13.5465(0.01×)	ee
$\gamma\gamma$	1.7	5.4315	TwoGam
HCT	0.10178	0.3252	HCT

Table 2: Component and corresponding observed cross section (output from ConExc) for charmonium hadronic transition (HCT) processes.

Mode index	Final state	Observed cross section @ 4180 MeV (nb)	Referee of input line shape
79	$\pi^0 \pi^0 \psi(2S)$	0.00342491	BELLE PRL99, 142002 (2007)
91	$\pi^+ \pi^- \psi(2S)$	0.00684981	BELLE PRL99, 142002 (2007)
80	$\eta J/\psi$	0.0321958	BELLE PRD87, 051101(R) (2013)
81	$\pi^+ \pi^- h_c$	0.0122136	BESIII PRL111,242001 (2013)
82	$\pi^0 \pi^0 h_c$	0.00610681	BESIII PRL111,242001 (2013)
83	$K^+ K^- J/\psi$	0.000671349	BELLE PRD77, 011105(R) (2008)
84	$K_S^0 K_S^0 J/\psi$	0.000167837	BELLE PRD77, 011105(R) (2008)
90	$\pi^+ \pi^- J/\psi$	0.026767	BELLE PRL99, 182004 (2007)
99	$\pi^0 \pi^0 J/\psi$	0.0133835	BELLE PRL99, 182004 (2007)
sum		0.101780616	

3 Event Selection

At $E_{cm} = 4.178\text{GeV}$, pairs of $D_s D_s^*$ are produced, and the D_s^* decays to either $D_s \gamma$ or $D_s \pi^0$. We use double tag method to select our signal events.

3.1 Tracking, PID, $\pi^0/\eta^{(\prime)}$ and K_S^0 Reconstruction

D_s candidates are built from K^\pm , π^\pm , $\pi^0/\eta^{(0)}$ and K_S^0 . The selections of the particles to build D_s candidates are performed with DTagAlg-00-01-05 package with the default setting, which are summarized below.

- Tracking:

- The properties of charged tracks are determined based on the MDC information. Charged track candidates must satisfy:

- $|\cos\theta| < 0.93$.

- $|dr| < 1\text{cm}$ and $|dz| < 10\text{cm}$,

where $|dr|$ and $|dz|$ are defined as the one reconstructed minus the interaction point.

- Particle ID:

- Charged tracks are identified as pion or kaon with Particle Identification (PID), which is implemented by combining the information of the energy loss (dE/dx) in MDC and the time-of-flight measured from the TOF system. Kaon and Pion are identified with the requirements that

- $\text{Prob}(K) > 0.00$ and $\text{Prob}(K) > \text{Prob}(\pi)$ for K ,

- $\text{Prob}(\pi) > 0.00$ and $\text{Prob}(\pi) > \text{Prob}(K)$ for π , where $\text{Prob}(X)$ is the probability of hypothesis X, X can be π or K .

- π^0/η selection: π^0 candidates are reconstructed through $\pi^0 \rightarrow \gamma\gamma$ with package of PioEtaToGGRecAlg.

The photons are reconstructed as energy showers on the EMC. We require:

- Minimum energy for barrel showers ($|\cos\theta| < 0.8$): $E_{min} > 25\text{MeV}/c^2$,

- Minimum energy for endcap showers ($0.86 < |\cos\theta| < 0.92$): $E_{min} > 50\text{MeV}/c^2$,

- Shower within other $|\cos\theta|$ regions are rejected.

- EMC time requirements for events with at least one charged track detected: $0 \leq t \leq 14(50\text{ns})$,

Then we perform a constrained fit on the photon pairs to the nominal π^0/η mass and require:

- The unconstrained invariant mass for π^0 : $0.115 < M(\gamma\gamma) < 0.015\text{GeV}/c^2$,

- The unconstrained invariant mass for η : $0.490 < M(\eta) < 0.580\text{GeV}/c^2$,

- Mass fit: $\chi^2_{1c} < 30$.

• η' selection: The η' candidates are reconstructed with $\pi^+\pi^-\eta$, the invariant mass for $\pi^+\pi^-\eta$ is required to fall into the range of $[0.938, 0.978]\text{GeV}^2$.

• K_S^0 selection: K_S^0 candidates are reconstructed using VeeVertexAlg package with two opposite charged tracks with requiring:

- $|\cos\theta| < 0.93$

- $|dz| < 20\text{cm}$

For each pair of tracks, a constrained vertex fit is performed and the track parameters' results are used to get the invariant mass $M(K_S^0)$. Then the decay length of K_S^0 is obtained with second vertex fit by the SecondVertexFit package. For K_S^0 selection, we require:

- $0.487\text{GeV}/c^2 < M(K_S^0) < 0.511\text{GeV}/c^2$.

- Significance of the K_S^0 decay length has two standard deviations.

• D_s selection: According to the MC study on D_s reconstruction (BESSIII-DocDB-380), the D_s candidates fall into the mass window of $1.90 < m_{D_s} < 2.03\text{GeV}/c^2$ and the corresponding M_{rec} satisfied $2.051 < M_{rec} < 2.180\text{GeV}/c^2$ are retained for further study. In which, the definition of M_{rec} is

$$M_{rec} = \sqrt{(E_{cm} - \sqrt{p_{D_s}^2 + m_{D_s}^2})^2 - |\vec{p}_{cm} - \vec{p}_{D_s}|^2}, \quad (1)$$

where E_{cm} is the energy of initial state, calculated from the beam energy [2], \vec{p}_{D_s} is the momentum of D_s candidate, m_{D_s} is D_s mass quoted from PDG [3] and \vec{p}_{cm} and \vec{p}_{D_s} are four-momentum of initial state and the decay products of a D_s candidate, respectively.

3.2 Single Tag Selection

After K^\pm , K_S^0 , π^\pm and γ are identified, hadronic D_s decays can be reconstructed with the DTag package. 8 tag modes are used:

$D_s^- \rightarrow K^+ K^- \pi^-$, $D_s^- \rightarrow K_S^0 K^-$, $D_s^- \rightarrow K_S^0 K^- \pi^+ \pi^-$, $D_s^- \rightarrow K^- \pi^+ \pi^-$, $D_s^- \rightarrow K_S^0 K^+ \pi^- \pi^-$, $D_s^- \rightarrow \pi^+ \pi^- \pi^-$, $D_s^- \rightarrow \eta'_{\pi^+ \pi^- \eta \gamma \gamma}$, $D_s^- \rightarrow K^+ K^- \pi^- \pi^0$.

Table 3: The ST yields(Y_{ST}) and ST efficiencies(ϵ_{ST}). The mass windows use the results in Ref. [4]

Tag mode	Mass window(GeV)	Y_{ST}	$\epsilon_{ST}(\%)$
$D_s^- \rightarrow K_S^0 K^-$	[1.948, 1.991]	958648 ± 1283	48.81 ± 0.07
$D_s^- \rightarrow K^+ K^- \pi^-$	[1.900, 2.030]	4064239 ± 2905	40.20 ± 0.03
$D_s^- \rightarrow K^+ K^- \pi^- \pi^0$	[1.947, 1.982]	1164312 ± 3430	10.56 ± 0.03
$D_s^- \rightarrow K_S^0 K^- \pi^+ \pi^-$	[1.958, 1.980]	233843 ± 1468	19.19 ± 0.12
$D_s^- \rightarrow K_S^0 K^+ \pi^- \pi^-$	[1.953, 1.983]	485855 ± 1313	22.59 ± 0.06
$D_s^- \rightarrow \pi^- \pi^- \pi^+$	[1.952, 1.984]	1159359 ± 3356	56.78 ± 0.16
$D_s^- \rightarrow \pi^- \eta' \pi^+ \pi^- \pi^- \eta_{\gamma\gamma}$	[1.940, 1.996]	251617 ± 737	20.26 ± 0.06
$D_s^- \rightarrow K^- \pi^+ \pi^-$	[1.953, 1.983]	500079 ± 2870	46.83 ± 0.27

In the selection of tag D_s , for multiple candidates, the best candidate is chosen with M_{rec} closest to mass of D_s^* in PDF [7]. To further remove the background associated with the larger number of soft $\pi^\pm(\pi^0)$ from D_s^* decays, candidates are voted if the momentum of $\pi^\pm(\pi^0)$ is less than $0.1 GeV$.

The single tag(ST) yields are extracted from the fits to the D_s invariant mass distributions, as shown in Fig.2. In the fit, the mass windows of the tag modes are set to be the same as the Ref. [4]. The signal shape is modeled as MC shape convoluted with a Gaussian function, while background is parameterized as the 2nd-order Chebychev polynomial. The corresponding ST efficiencies are estimated from generic MC. The ST yields(Y_{ST}) and ST efficiencies(ϵ_{ST}) are listed in Tab.3

With the tagged D_s meson, the signal D_s is reconstructed with the remaining good tracks and good showers. The momentum of $\pi^\pm(\pi^0)$ is required to be larger than $100 MeV/c^2$ to suppress the background of $D^* \rightarrow D\pi$. Only the D_s candidate with invariant mass falls into $[1.87, 2.06] GeV/c^2$ are selected.

For every candidate of D_s decays, all tracks at signal side and tag side as well as gamma from D_s^* are added to apply kinematic fitting. 5 constraints are added in kinematic fitting: four-momentum of $D_s D_s^*$, mass of D_s^* . Then we select the candidate with minimum χ_{5c}^2 .

The candidates satisfy:

$$- 1.95 GeV < m_{sig} < 1.985 GeV$$

$$- 1.95 GeV < m_{tag} < 1.985 GeV$$

$$- \chi_{5c}^2 < 50$$

are retained for amplitude analysis, where m_{sig} and m_{tag} refer to mass of D_s at signal side and tag side respectively.

3.3 Background Analysis

We use generic MC to estimate the background. The background and signal shape of generic MC is shown in Fig.???. According to the luminosities of the data and the generic MC, after scaling the background sample to the data size, the background yields in Signal region is 11.8. Then the fit to the signal D_s invariant mass (m_{sig}) spectrum gives the background yield in Signal region is 11.3 ± 3.9 , shown as in Fig.3. The background level in MC is then consistent with the data. In the fit, the signal shape is the MC shape convoluted with a Gaussian function and the background is the MC shape.

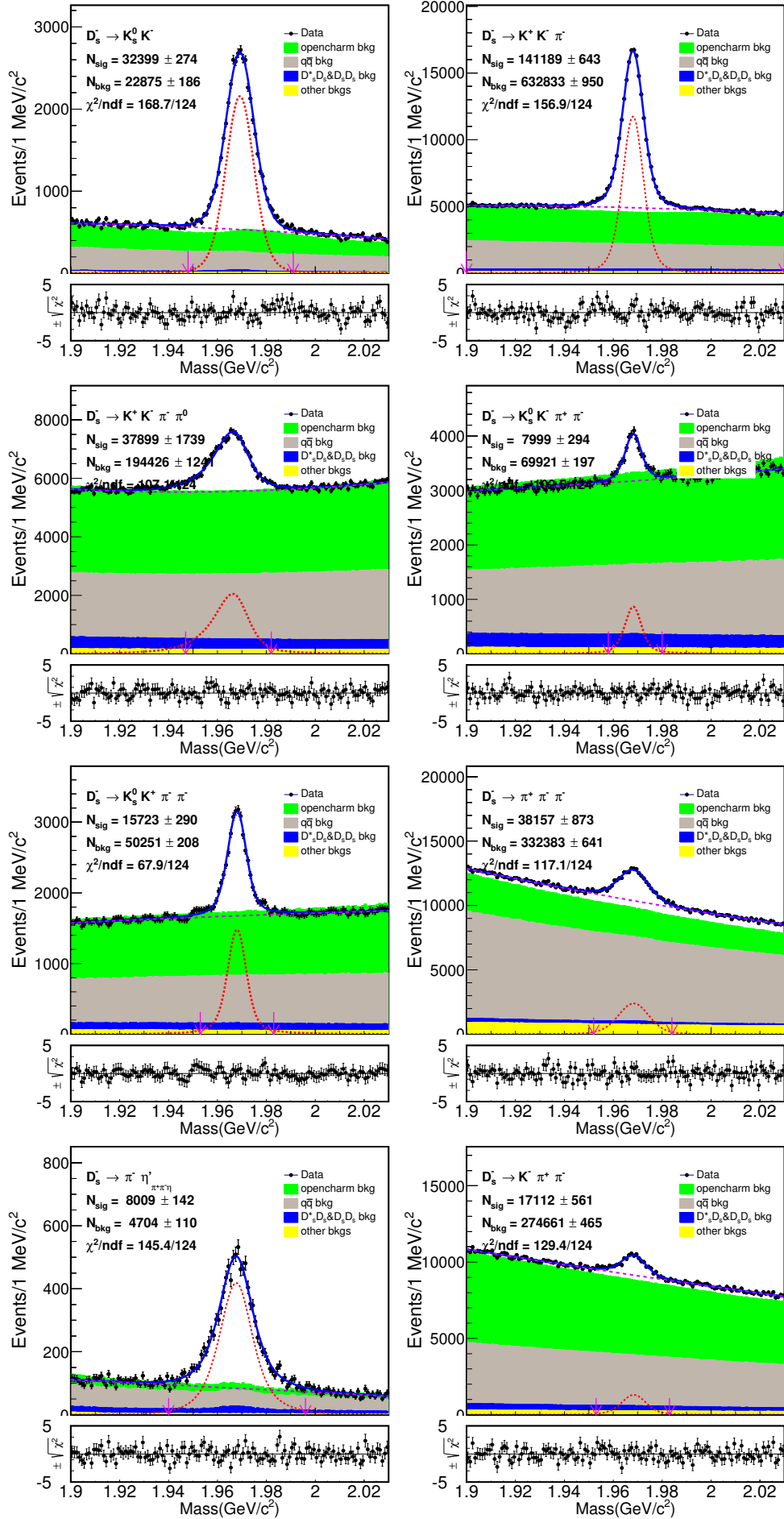


Figure 2: D_s Mass fits from data. The points with error bars are data, and the blue line is the fit. Red short-dashed lines are signal, violet long-dashed lines are background. The red arrows denote the signal region.

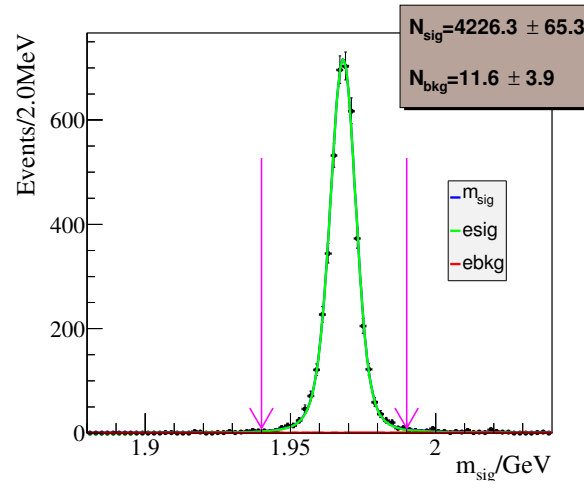


Figure 3: The fit to m_{sig} for data after selections, the area between the purple arrows is the signal area of the sample for the amplitude analysis.

4 Model Independent Partial Wave Analysis

In the K^+K^- threshold both $a_0(980)$ and $f_0(980)$ can be present, and both resonances have very similar parameters which suffer from large uncertainties. In this section we obtain model-independent information on the K^+K^-S wave by performing a MIPPPWA(model indendent partial wave analysis) in the K^+K^- threshold region.

4.1 Signal Candidate Selection

As MIPWA need more data events, we do not require D_s^+ and D_s^- appear in pairs. Before selecting the best candidate, we vote the candidates with $\pi^\pm(\pi^0)$ whose momentum is less than 0.1GeV to remove soft $\pi^\pm(\pi^0)$ from D^* decays. For every candidates of D_s decays, all tracks at signal side are added to apply kinematic fitting. Only mass of D_s from signal side is constrained. Then we select the candidate with minimum χ^2_{1c} .

4.2 Background Analysis

In order to further suppress the background, the multiple analysis method (MVA) is used. We train MVA methods separately with different sets of variables for the two event categories depending on the D_s^+ origin. These two categories of events are selected in a $M_{rec} - \Delta M$ 2D plane shown in Fig.4:

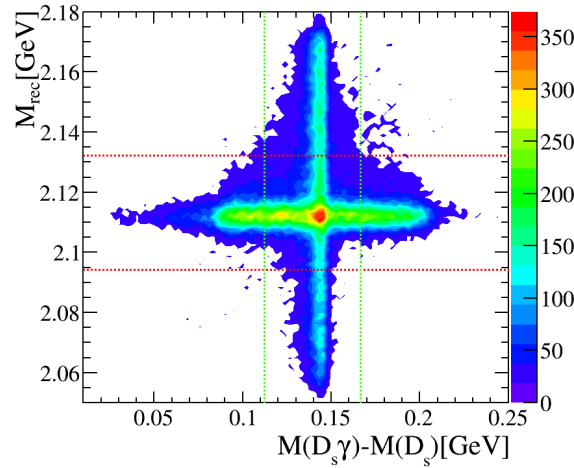


Figure 4: Two dimensional plane of $\Delta M \equiv M(D_s^+ \gamma) - M(D_s^+)$ versus M_{rec} from the simulated $D_s^+ \rightarrow K^+ K^- \pi^+$ decays. The red(green) dashed lines mark the mass window for the D_s^+ Cat. #0(Cat. #1) around the $M_{rec}(\Delta M)$ peak.

- Cat. #0: Direct D_s^+ . We use the following variables whose distributions for signal and background are shown in Fig.5,

1. M_{rec} ,
 2. P_{rest} , defined as the total momentum of the tracks and neutrals in the rest of event (not part of the $D_s^+ \rightarrow K^+ K^- \pi^+$ candidate),
 3. N_{tracks} , defined as the total number of tracks and neutrals in an event.
- Cat. #1: Indirect D_s^+ . We use the following variables whose distributions for signal and background are shown in Fig.6,
1. ΔM ,
 2. M'_{rec} , defined as $M'_{rec} = \sqrt{(E_{cm} - \sqrt{p_{D_s\gamma}^2 + m_{D_s^*}^2})^2 - p_{D_s\gamma}^2}$, with $p_{D_s\gamma}$ as the momentum of the $D_s\gamma$ combination, $m_{D_s^*}$ as the nominal D_s^* mass,
 3. E_γ , defined as the energy of gamma from D_s^* .

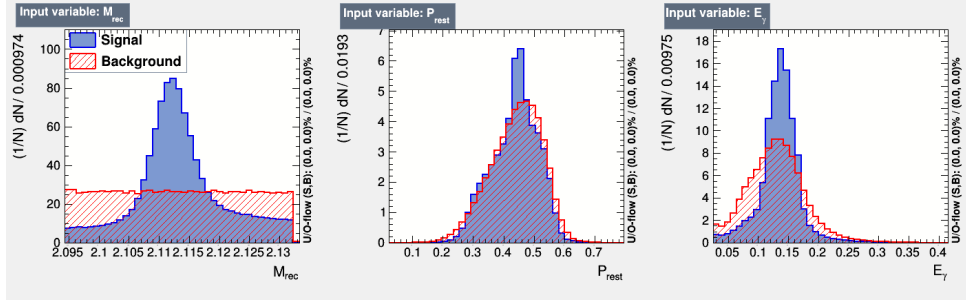


Figure 5: For event Cat. #0, distributions of MVA variables from simulated signal decays and background events.

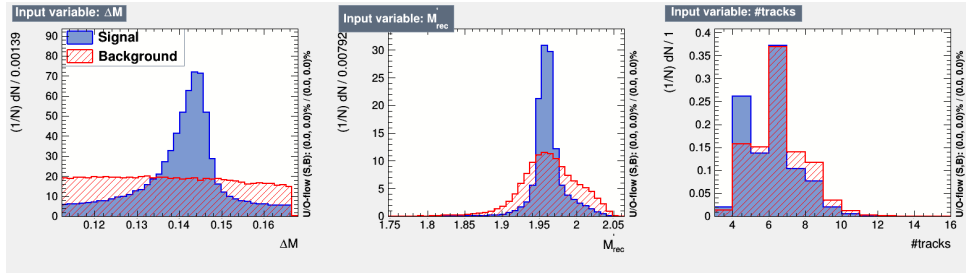


Figure 6: For event Cat. #1, distributions of MVA variables from simulated signal decays and background events.

As the results shown in Fig.7, this BDTG training and test samples are well matched. For event Cat. #0 (Cat. #1), the sample with BDTG value larger than 0.33(0.65) is retained for further study.

After applying the BDTG requirement, the background shows no obviously peak around the region of $[1.95, 1.982] \text{ GeV}$ (Signal region), which are shown in Fig.8. The fit to the signal D_s invariant mass

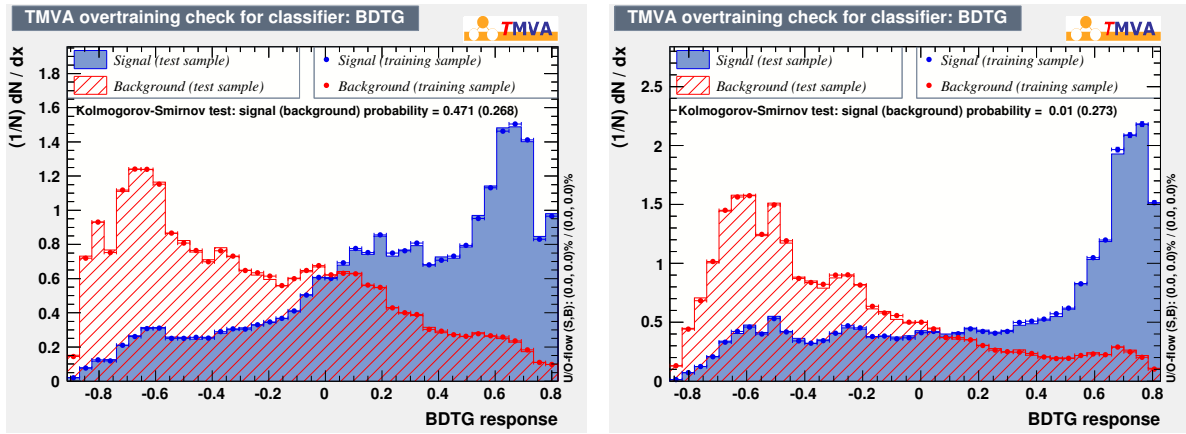


Figure 7: The comparisons between the training and test samples.

- 1 $(M_{D_s^2})$ spectrum gives the background yield in Signal region is 73.6 ± 18.7 , shown as in Fig.9. In the fit,
- 2 the signal shape is the MC shape convoluted with a Gaussian function and the background is described
- 3 with 1st-order Chebychev polynomial.

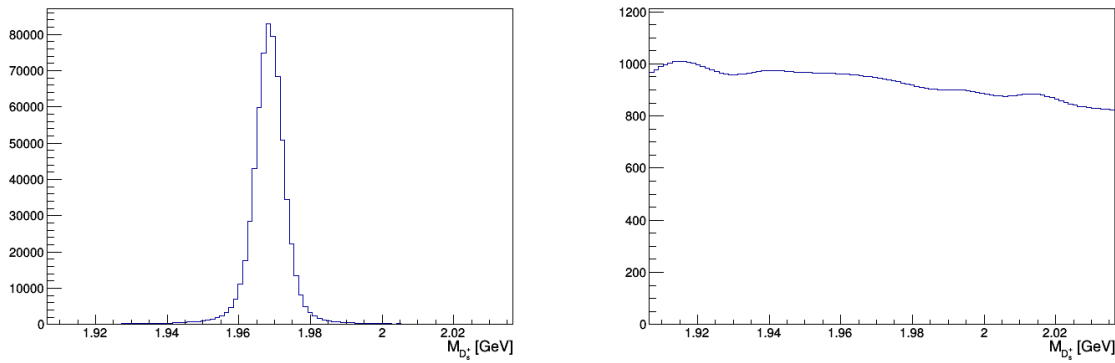


Figure 8: The signal and background distributions from generic MC after BDTG requirement.

- 4 The projections of the "Sideband" ($1.90 < M(D_s) < 1.95 \text{ GeV}$ and $1.985 < M(D_s) < 2.03 \text{ GeV}$) from
- 5 data and generic MC after signal events removed are shown in Fig.10. The corresponding plots agree
- 6 well.
- 7 Thus the generic MC sample with signal events removed is used to subtract the background in
- 8 MIPWA.

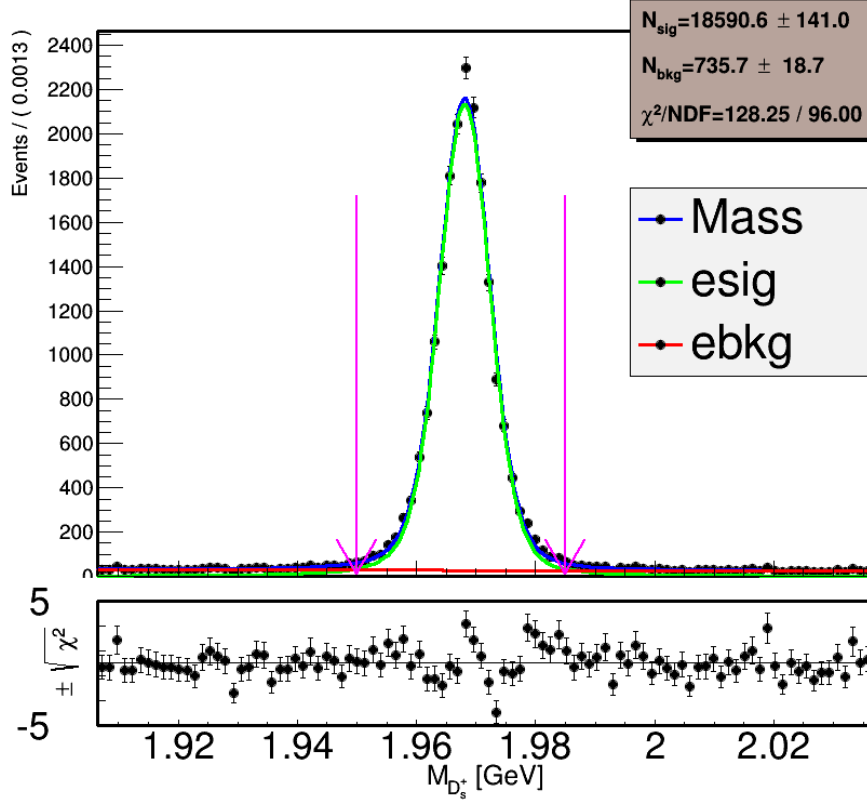


Figure 9: The fit to the signal D_s invariant mass ($M_{D_s^*}$) spectrum after BDTG requirement, the area between the pink arrows is the signal area of the sample for MIPWA.

4.3 MIPWA method

Let N be the number of events for a given mass interval $I = [m_{K^+K^-}; m_{K^+K^-} + dm_{K^+K^-}]$. We write the corresponding angular distributions in terms of the appropriate spherical harmonic functions as

$$\frac{dN}{d\cos\theta} = 2\pi \sum_{k=0}^L \langle Y_k^0 \rangle Y_k^0(\cos\theta), \quad (2)$$

where $L = 2\ell_{max}$, and ℓ_{max} is the maximum orbital angular momentum quantum number required to describe the K^+K^- system at $m_{K^+K^-}$ (e.g. $\ell_{max} = 1$ for S-, P-wave description); θ is the angle between the K^+ direction in the K^+K^- system in the D_s^* rest frame. The normalizations are such that

$$\int_{-1}^1 Y_k^0(\cos\theta) Y_j^0(\cos\theta) d\cos\theta = \frac{\delta_{kj}}{2\pi}, \quad (3)$$

and it is assumed that the distribution $\frac{dN}{d\cos\theta}$ has been efficiency corrected and background subtracted.

Using this orthogonality condition, the coefficients in the expansion are obtained from

$$\langle Y_k^0 \rangle = \int_{-1}^1 \frac{dN}{d\cos\theta} d\cos\theta, \quad (4)$$

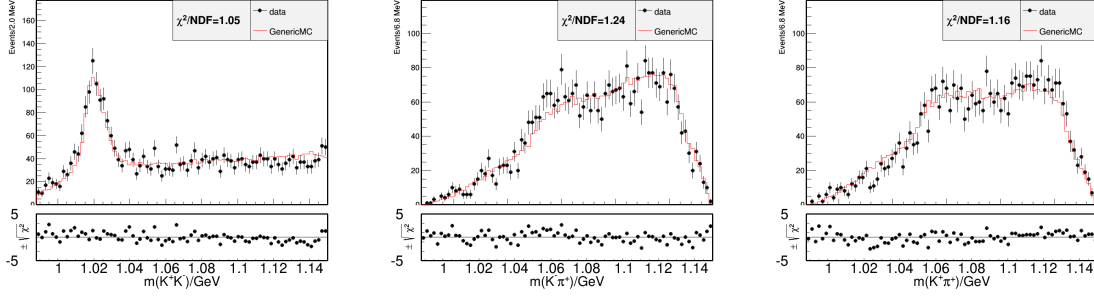


Figure 10: The projections of $m(K^+K^-)$, $m(K^-\pi^+)$, $m(K^+\pi^+)$ from "Sideband" for data(dots with error bars) and generic MC after signal events removed (red histogram) after BDTG requirement.

where the integral is given, to a good approximation, by $\sum_{n=1}^N Y_k^0(\cos \theta_n)$, where θ_n is the value of θ for the n -th event.

Fig. 11 shows the K^+K^- mass spectrum up to 1.15 GeV weighted by $Y_k^0(\cos \theta) = \sqrt{(2k+1)/(4\pi)} P_k(\cos \theta)$ for $k=0, 1$, and 2, where P_k is the Legendre polynomial function of order k . These distributions are corrected for efficiency and phase space, and background is subtracted using background from generic MC after BDTG requirement.

The number of events N for the mass interval I can be expressed also in terms of the partial-wave amplitudes describing the K^+K^- system. Assuming that only S- and P-wave amplitudes are necessary in this limited region, we can write:

$$\frac{dN}{d\cos\theta} = 2\pi |S Y_0^0(\cos\theta) + P Y_1^0(\cos\theta)|^2. \quad (5)$$

By comparing Eqa. 2 and 5, we obtain

$$\begin{aligned} \sqrt{4\pi} \langle Y_0^0 \rangle &= |S|^2 + |P|^2, \\ \sqrt{4\pi} \langle Y_2^0 \rangle &= \frac{2}{\sqrt{5}} |P|^2, \end{aligned} \quad (6)$$

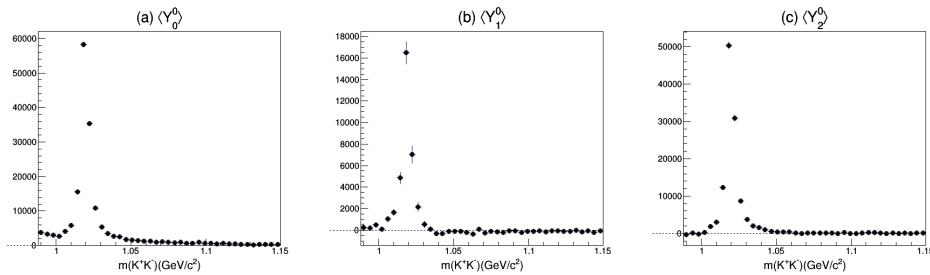


Figure 11: K^+K^- mass spectrum in the threshold region weighted by (a) Y_0^0 , (b) Y_1^0 and (c) Y_2^0 , corrected for efficiency and phase space, and background subtracted.

The above system of equations can be solved in each interval of K^+K^- invariant mass for $|S|$ and $|P|$ and the resulting distributions are shown in Fig. 12.

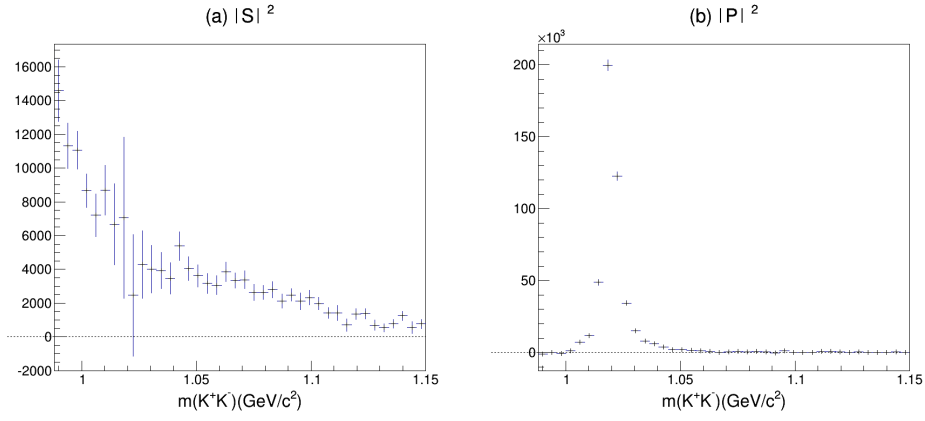


Figure 12: Squared (a) S- and (b) P-wave amplitudes

4.4 S-wave parameterization at the K^+K^- threshold

We empirically parameterize the $f_0(980)$ with the following function:

$$A_{f_0(980)/a_0(980)} = \frac{1}{m_0^2 - m^2 - im_0\Gamma_0\rho_{KK}}, \quad (7)$$

where $\rho_{KK} = 2p/m$, and obtain the following parameter values:

$$\begin{aligned} m_0 &= (0.919 \pm 0.006_{stat})GeV, \\ \Gamma_0 &= (0.272 \pm 0.020_{stat})GeV. \end{aligned} \quad (8)$$

The errors are statistical only. The fit result are shown in Fig.13.

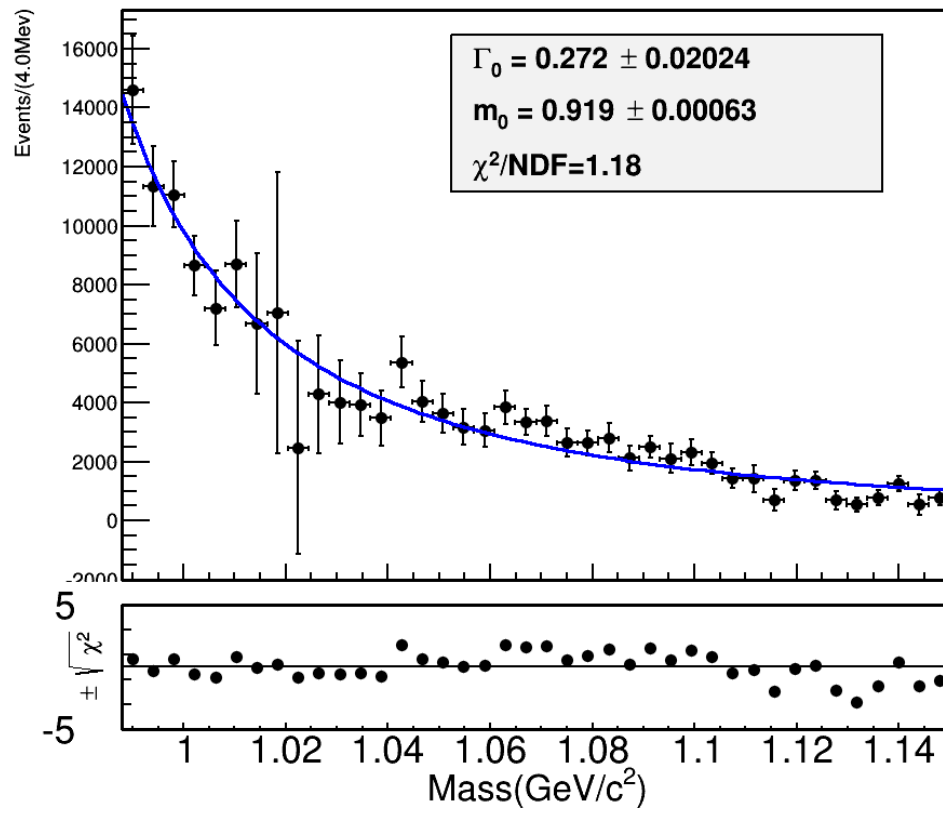


Figure 13: Fit of squared S-wave amplitudes. the curves result from the fit described in the text.

5 Amplitude Analysis

5.1 Fit Method

The method used in amplitude analysis is the same as the Ref. [5]. In this section, we briefly review the amplitude analysis method used in this analysis.

The relative magnitudes and phases of the partial waves and the mass and width of intermediate resonances are determined by a maximum-likelihood fit to the data selected. The formulas are constructed with covariant tensors [6].

Since there are three final state particles, only one possible resonant state is allowed in any intermediate process. Thus the amplitude of the n^{th} intermediate state (A_n) is,

$$A_n = P_n S_n F_n^r F_n^D, \quad (9)$$

where S_n and $F_n^{r(D)}$ are the spin factor and the Blatt-Weisskopf barriers of the intermediate state (the D_s meson), respectively. P_n is the propagator of the intermediate resonance. For a decay process $a \rightarrow bc$, $s_{a/b/c}$ is denoted to be the invariant mass square of the particle a/b/c, and q is denoted as the magnitude of the momentum daughter particle in the rest system of a

$$q = \sqrt{\frac{(s_a + s_b + s_c)^2}{4s_a} - s_b}. \quad (10)$$

Then for $K^*(892)^0$, $\Phi(1020)^0$, $K_0^*(1430)^0$ and $f_0(1710)$, they are parameterized as a RBW,

$$P = \frac{1}{(m_0^2 - s_a - im_0\Gamma(m))}, \quad (11)$$

$$\Gamma(m) = \Gamma_0 \left(\frac{q}{q_0}\right)^3 \left(\frac{m_0}{m}\right) (F^r)^2,$$

where m_0 and Γ_0 are the mass and the width of the intermediate resonances, and are fixed to the PDG values [7] except the mass and the width of $f_0(1370)$. The mass and width of $f_0(1370)$ are fixed to Ref. [8]. $K_0^*(1430)^0$ is parameterized with Flatte formula:

$$P_{K_0^*(1430)^0} = \frac{1}{M^2 - s - i(g_1\rho_{K\pi}(s) + g_2\rho_{\eta'K}(s))}, \quad (12)$$

where s is the $K^-\pi^+$ invariant mass squared, $\rho_{K\pi}(s)$ and $\rho_{\eta'K}(s)$ are Lorentz invariant PHSP factor, and $g_{1,2}$ are coupling constants to the corresponding final state. The parameters of $K_0^*(1430)^0$ are fixed to values measured by CLEO [9]. For resonance $f_0(980)$ & $a_0(980)$, the RBW form 7 is used to describe the propagator and the values of parameters are fixed to the values in 8.

The Blatt-Weisskopf barriers are given by

$$F_n = 1, (S\text{wave}),$$

$$F_n = \sqrt{\frac{z_0^2 + 1}{z^2 + 1}}, (P\text{wave}), \quad (13)$$

$$F_n = \sqrt{\frac{z_0^4 + 3z_0^2 + 9}{z^4 + 3z^2 + 9}}, (D\text{wave}),$$

where z and z_0 are qR and q_0R , respectively. The R is the effective radius of the intermediate state or D_s meson and set to 3.0GeV^{-1} for intermediate states and 5.0GeV^{-1} for D_s meson [5], respectively.

As the limit of the phase space, we only consider the states with angular momenta no more than 2. As discussed in [10], the spin factor is,

$$\begin{aligned} S_n &= 1, (S\text{ wave}), \\ S_n &= \tilde{T}^{(1)\mu}(D_s) \tilde{t}_\mu^{(1)}(R), (P\text{ wave}), \\ S_n &= \tilde{T}^{(2)\mu}(D_s) \tilde{t}_\mu^{(2)}(R), (D\text{ wave}), \end{aligned} \quad (14)$$

where the $\tilde{T}^{(1)\mu}(D_s)$ ($\tilde{T}^{(2)\mu}(D_s)$) and $\tilde{t}_\mu^{(1)}(R)$ ($\tilde{t}_\mu^{(2)}(R)$) are the same defined in Ref. [6].

The total amplitude M is then the coherent sum of the amplitudes of intermediate processes, $M = \sum c_n A_n$, where $c_n = \rho_n e^{i\phi_n}$, is the corresponding complex coefficient. The magnitude ρ_n and phase ϕ_n are determined by the amplitude analysis. The signal PDF $f_S(p_j)$ is given by

$$f_S(p_j) = \frac{\epsilon(p_j) |M(p_j)|^2 R_3(p_j)}{\int \epsilon(p_j) |M(p_j)|^2 R_3(p_j) dp_j}, \quad (15)$$

where $\epsilon(p_j)$ is the detection efficiency parameterized in terms of the final four-momenta p_j . The index j refers to the different particles in the final states. $R_3(p_j) dp_j$ is the standard element of the three-body phase space. The normalization integral is determined by a MC technique,

$$\int \epsilon(p_j) |M(p_j)|^2 R_3(p_j) dp_j = \frac{1}{N_{MC}} \sum_{k_{MC}}^{N_{MC}} \frac{|M(p_j^{k_{MC}})|^2}{|M^{gen}(p_j^{k_{MC}})|^2}, \quad (16)$$

where k_{MC} is the index of the k_{MC}^{th} event of the MC sample and N_{MC} is the number of the selected MC events. In this analysis, a signal MC sample with about 2 million events is used in the normalization integral calculation. $M^{gen}(p_j)$ is the PDF function used to generate the MC samples in MC integration. Firstly, the PHSP MC are used in MC integration. $M^{gen}(p_j)$ is a constant overall the phase space. Then with result obtained from the fit to data, the signal MC is then generated and used in MC integration. In the numerator of Eq. 15, $\epsilon(p_j)$ is independent of the fitted variables, so it is regarded as a constant term in the fit.

Since there is only 0.3% background in the data sample, the contribution from the background is ignored in the likelihood calculation:

$$\ln L = \sum_k^{N_{data}} \ln f_S(p_j^k), \quad (17)$$

where N_{data} is the number of candidate events in data.

5.2 Fit Fraction

The fit fractions of the individual amplitudes are calculated according to the fit results and are compared to the other measurements. In the calculation, a phase space(PHSP) MC with neither detector

1 acceptance nor resolution involved is used. The fit fraction for an amplitude is defined as

$$FF(n) = \frac{\sum_{k=1}^{N_{gen}} |A_n|^2}{\sum_{k=1}^{N_{gen}} |M(p_j^k)|^2}, \quad (18)$$

2 where $N_{gen} = 2000000$, is the number of the PHSP MC events in this analysis.

3 To estimate the statistical uncertainties of the fit fractions, we repeat the calculation of fit fractions
4 by randomly varying the fitted parameters according to the error matrix. Then, for each amplitude, we
5 fit the resulting distribution with a Gaussian function, whose width gives the corresponding statistical
6 uncertainty.

7 5.3 Fit Result

8 The Dalitz plot of $m^2(K^+K^-)$ versus $m^2(K^-\pi^+)$ is shown in Fig.14. In the plot, we can see a clear
9 peak of $K^*(892)^0$ and $\phi(1020)^0$. In the fit, the magnitude and phase of the amplitude $D_s^+ \rightarrow K^*(892)^0 K^+$
10 is fixed to 1.0 and 0.0, and the magnitudes and phases of the amplitudes are allowed to float.

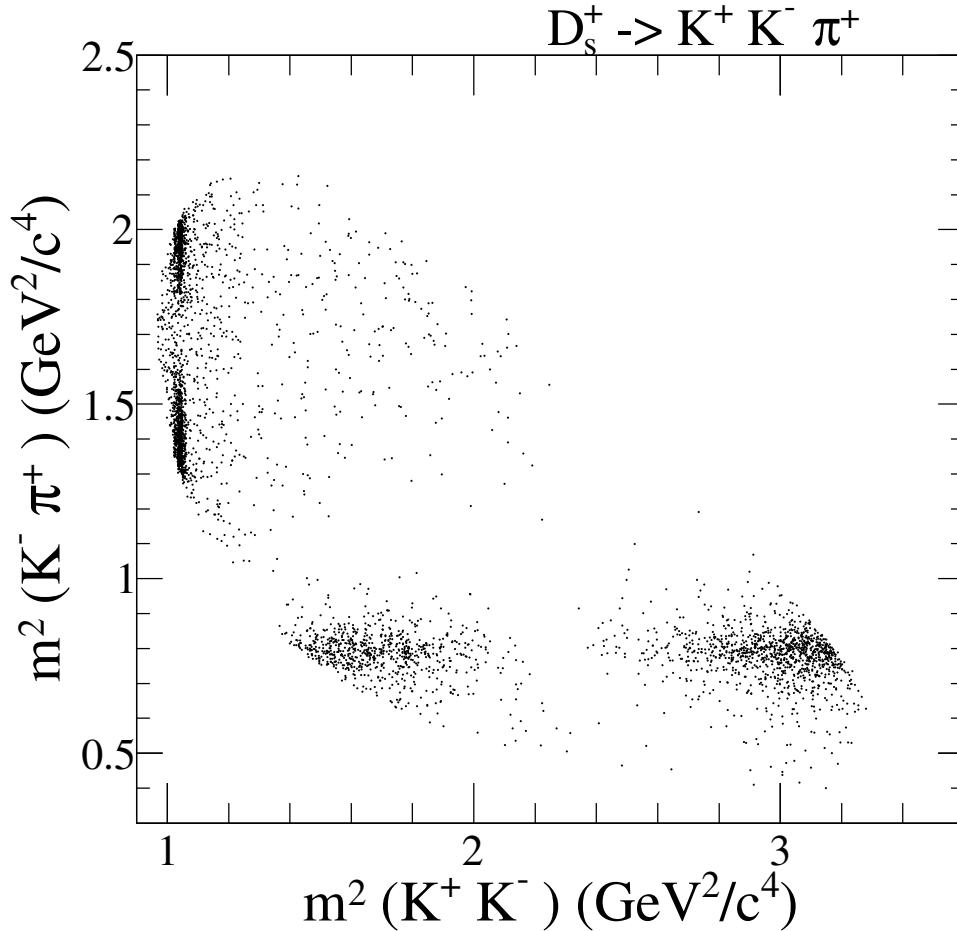


Figure 14: The plot of $m^2(K^+K^-)$ versus $m^2(K^-\pi^+)$ after event selection.

Table 4: The $\Delta \ln L$, Δn_{par} , and the statistical significance for each amplitude

Amplitude	$\Delta \ln L$	Δn_{par}	Stat. significance
$D_s^+ \rightarrow \bar{K}^*(892)^0 K^+$	1959.3	2	>20
$D_s^+ \rightarrow \phi(1020)\pi^+$	2303.3	2	>20
$D_s^+ \rightarrow f_0(980)\pi^+ / a_0(980)\pi^+$	270.5	2	>20
$D_s^+ \rightarrow \bar{K}_0^*(1430)^0 K^+$	39.4	2	8.6
$D_s^+ \rightarrow f_0(1370)\pi^+$	22.5	2	6.4
$D_s^+ \rightarrow f_0(1710)\pi^+$	44.7	2	9.2

Table 5: The magnitudes, phases and fit fractions for the six amplitudes

Amplitude	Magnitude	Phase	Fit fractions(%)
$D_s^+ \rightarrow \bar{K}^*(892)^0 K^+$	1.0(fixed)	0.0(fixed)	48.3±0.9
$D_s^+ \rightarrow \phi(1020)\pi^+$	1.09±0.02	6.22±0.07	40.5±0.7
$D_s^+ \rightarrow f_0(980)\pi^+ / a_0(980)\pi^+$	2.88±0.14	4.77±0.07	19.3±1.7
$D_s^+ \rightarrow \bar{K}_0^*(1430)^0 K^+$	1.26±0.14	2.91±0.20	3.0±0.6
$D_s^+ \rightarrow f_0(1710)\pi^+$	0.79±0.08	1.02±0.12	1.9±0.4
$D_s^+ \rightarrow f_0(1370)\pi^+$	0.58±0.08	0.59±0.17	1.2±0.4

With the requiring the statistical significance larger than 5 standard deviations, there are 6 intermediate process, $D_s^+ \rightarrow \bar{K}^*(892)^0 K^+$, $D_s^+ \rightarrow \phi(1020)\pi^+$, $D_s^+ \rightarrow f_0(980)\pi^+ / a_0(980)\pi^+$, $D_s^+ \rightarrow \bar{K}_0^*(1430)^0 K^+$, $D_s^+ \rightarrow f_0(1370)\pi^+$, $D_s^+ \rightarrow f_0(1710)\pi^+$ are retained in final result. The statistical significance of the three amplitudes in final result are also checked.

With one amplitude dropped and the fit repeated, compared with the nominal fit the likelihood shift($\Delta \ln L$) and the number of freedom degree shift(Δn_{par}) are then corresponding to the statistical significance. The detail $\Delta \ln L$, Δn_{par} , and the statistical significance for each amplitude are listed in Tab.4.

The detail magnitudes, phases and fit fractions for the six amplitudes are listed in Tab. 5.

The Dalitz plot projections are shown in Fig.15.

The goodness of the nominal fit is $\chi^2 = 290.1/280 = 1.04$.

5.4 Sytematic Uncertainties

Systematic uncertainties takein account:

- I Variation of resonance masses and widths within 1σ error.

- For $f_0(980)/a_0(980)$, the mass and width are shifted within errors from Eq.8 in model independent PWA part.

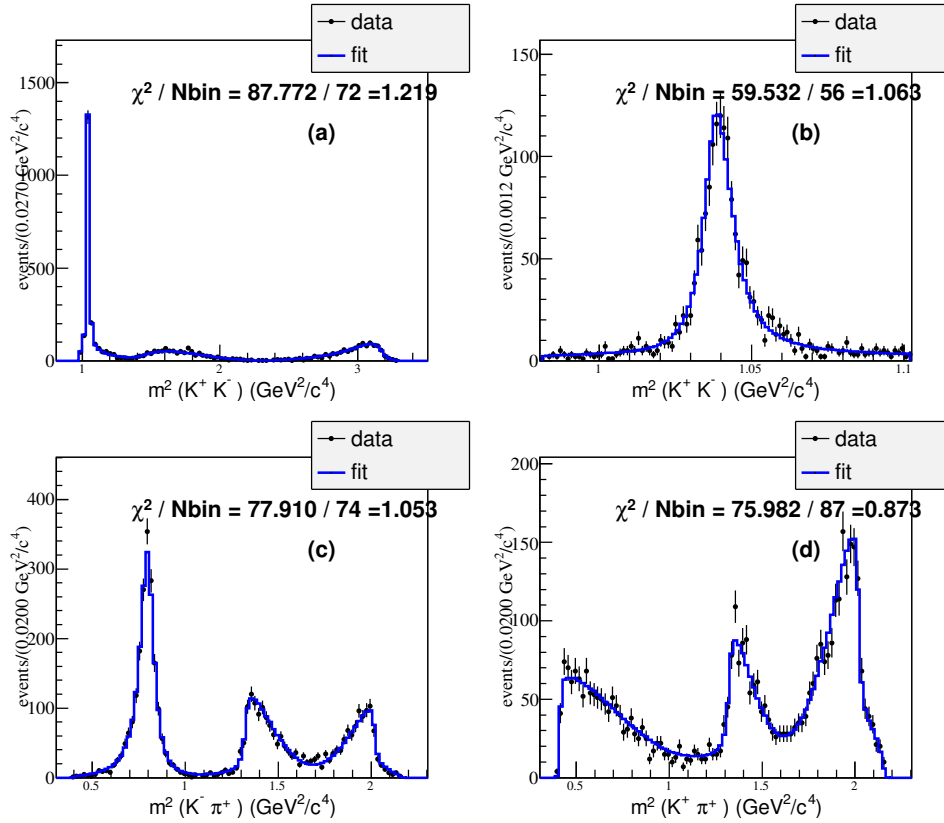


Figure 15: $D_s^+ \rightarrow K^+ K^- \pi^+$: Dalitz plot projections from the nominal fit. The data are represented by points with error bars, the fit results by the histograms.

- For $f_0(1370)$, the mass and width are shifted within errors from [8].
- For other states, errors used here are taken from PDG [7].
- II Variation of the effective radius of Blatt-Weisskopf Barrier within the range $[1.0, 5.0] \text{ GeV}^{-1}$ for intermediate resonances and $[3.0, 7.0] \text{ GeV}^{-1}$ for D_s meson.
- III Fit bias. The possible bias is given by the result from pull distribution check. With the results obtained from the fit, the signal MC samples are generated with the same size of the data. In this analysis, 300 MC samples with the size equaling to data are used to perform the pull distribution check. The results are listed in Tab.6. The corresponding plots are shown in Fig.16, Fig.17 and Fig.18.

Thus, the detail results of the systematic uncertainties are summarized in Tab.7. The final results of the amplitude analysis are then listed in Tab.9.

Below is a comparison between BABAR, CLEO-c and this analysis.

Table 6: The results of pull distribution checks for the magnitudes, phases and fit fractions for the amplitudes

Amplitude	Phase		Magnitude		Fit fraction	
	mean	width	mean	width	mean	width
$D_s^+ \rightarrow \bar{K}^*(892)^0 K^+$					-0.13 ± 0.04	0.98 ± 0.03
$D_s^+ \rightarrow \phi(1020)\pi^+$	-0.04 ± 0.05	1.00 ± 0.03	0.07 ± 0.04	0.95 ± 0.03	0.01 ± 0.04	0.95 ± 0.03
$D_s^+ \rightarrow f_0(980)\pi^+ / a_0(980)\pi^+$	-0.07 ± 0.05	1.01 ± 0.03	0.07 ± 0.05	1.10 ± 0.04	0.02 ± 0.05	1.14 ± 0.04
$D_s^+ \rightarrow \bar{K}_0^*(1430)^0 K^+$	0.00 ± 0.05	1.11 ± 0.04	0.14 ± 0.04	0.95 ± 0.03	0.10 ± 0.04	0.99 ± 0.03
$D_s^+ \rightarrow f_0(1710)\pi^+$	0.00 ± 0.04	0.98 ± 0.03	0.08 ± 0.04	0.97 ± 0.03	0.01 ± 0.04	0.99 ± 0.03
$D_s^+ \rightarrow f_0(1370)\pi^+$	-0.11 ± 0.05	1.10 ± 0.04	0.21 ± 0.04	0.99 ± 0.03	0.15 ± 0.04	0.98 ± 0.03

Table 7: Systematic uncertainties on the ϕ and FFs for different amplitudes in units of the corresponding statistical uncertainties.

Amplitude		Source			
		I	II	III	Total
$D_s^+ \rightarrow \bar{K}^*(892)^0 K^+$	FF	0.32	0.29	0.13	0.46
$D_s^+ \rightarrow \phi(1020)\pi^+$	ϕ	0.49	0.10	0.06	0.51
	ρ	0.49	0.14	0.18	0.54
	FF	0.44	1.13	0.05	1.21
$D_s^+ \rightarrow f_0(980)\pi^+ / a_0(980)\pi^+$	ϕ	0.98	0.25	0.06	1.01
	ρ	1.11	0.17	0.10	1.13
	FF	1.16	0.15	0.06	1.17
$D_s^+ \rightarrow \bar{K}_0^*(1430)^0 K^+$	ϕ	1.02	0.48	0.09	1.13
	ρ	1.00	0.36	0.13	1.07
	FF	0.76	0.35	0.11	0.85
$D_s^+ \rightarrow f_0(1710)\pi^+$	ϕ	0.31	0.25	0.09	0.41
	ρ	1.17	1.23	0.07	1.70
	FF	0.71	1.21	0.05	1.41
$D_s^+ \rightarrow f_0(1370)\pi^+$	ϕ	2.66	0.27	0.11	2.67
	ρ	1.01	0.32	0.06	1.06
	FF	0.42	0.30	0.15	0.54

Table 8: The final results of the magnitudes, phases and fit fractions for the six amplitudes. The first and second uncertainties are the statistical and systematic uncertainties, respectively.

Amplitude	Magnitude	Phase	Fit fractions(%)
$D_s^+ \rightarrow \bar{K}^*(892)^0 K^+$	1.0(fixed)	0.0(fixed)	$48.3 \pm 0.9 \pm 0.4$
$D_s^+ \rightarrow \phi(1020)\pi^+$	$1.09 \pm 0.02 \pm 0.01$	$6.22 \pm 0.07 \pm 0.04$	$40.5 \pm 0.7 \pm 0.9$
$D_s^+ \rightarrow f_0(980)\pi^+ / a_0(980)\pi^+$	$2.88 \pm 0.14 \pm 0.16$	$4.77 \pm 0.07 \pm 0.07$	$19.3 \pm 1.7 \pm 2.0$
$D_s^+ \rightarrow \bar{K}_0^*(1430)^0 K^+$	$1.26 \pm 0.14 \pm 0.15$	$2.91 \pm 0.20 \pm 0.23$	$3.0 \pm 0.6 \pm 0.5$
$D_s^+ \rightarrow f_0(1710)\pi^+$	$0.79 \pm 0.08 \pm 0.14$	$1.02 \pm 0.12 \pm 0.05$	$1.9 \pm 0.4 \pm 0.6$
$D_s^+ \rightarrow f_0(1370)\pi^+$	$0.58 \pm 0.08 \pm 0.08$	$0.59 \pm 0.17 \pm 0.45$	$1.2 \pm 0.4 \pm 0.2$

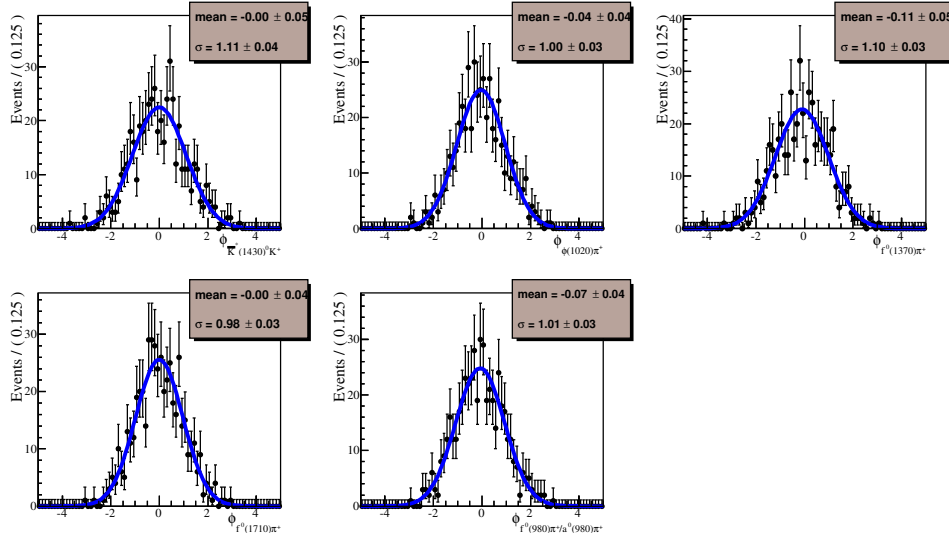


Figure 16: The pull distribution check results for phases of the amplitudes in the nominal fit model.

Table 9: Comparison between BABAR, CLEO-c and this analysis.

Amplitude	BABAR	CLEO-c	This Analysis
$D_s^+ \rightarrow \bar{K}^*(892)^0 K^+$	$47.9 \pm 0.5 \pm 0.5$	$47.4 \pm 1.5 \pm 0.4$	$48.3 \pm 0.9 \pm 0.4$
$D_s^+ \rightarrow \phi(1020)\pi^+$	$41.4 \pm 0.8 \pm 0.5$	$42.2 \pm 1.6 \pm 0.3$	$40.5 \pm 0.7 \pm 0.9$
$D_s^+ \rightarrow f_0(980)\pi^+ / a_0(980)\pi^+$	$16.4 \pm 0.7 \pm 2.0$	$28.2 \pm 1.9 \pm 1.8$	$19.3 \pm 1.7 \pm 2.0$
$D_s^+ \rightarrow \bar{K}_0^*(1430)^0 K^+$	$2.4 \pm 0.3 \pm 1.0$	$3.9 \pm 0.5 \pm 0.5$	$3.0 \pm 0.6 \pm 0.5$
$D_s^+ \rightarrow f_0(1710)\pi^+$	$1.1 \pm 0.1 \pm 0.1$	$3.4 \pm 0.5 \pm 0.3$	$1.9 \pm 0.4 \pm 0.6$
$D_s^+ \rightarrow f_0(1370)\pi^+$	$1.1 \pm 0.1 \pm 0.2$	$4.3 \pm 0.6 \pm 0.5$	$1.2 \pm 0.4 \pm 0.2$
$\sum FF(\%)$	$110.2 \pm 0.6 \pm 2.0$	$129.5 \pm 4.4 \pm 2.0$	$114.2 \pm 1.7 \pm 2.3$
χ^2/NDF	$\frac{2843}{2305-14} = 1.2$	$\frac{178}{117} = 1.5$	$\frac{290}{291-10-1} = 1.04$
Events	96307 ± 369	$14400(\text{purity}85\%)$	$4485(\text{purity}99.7\%)$

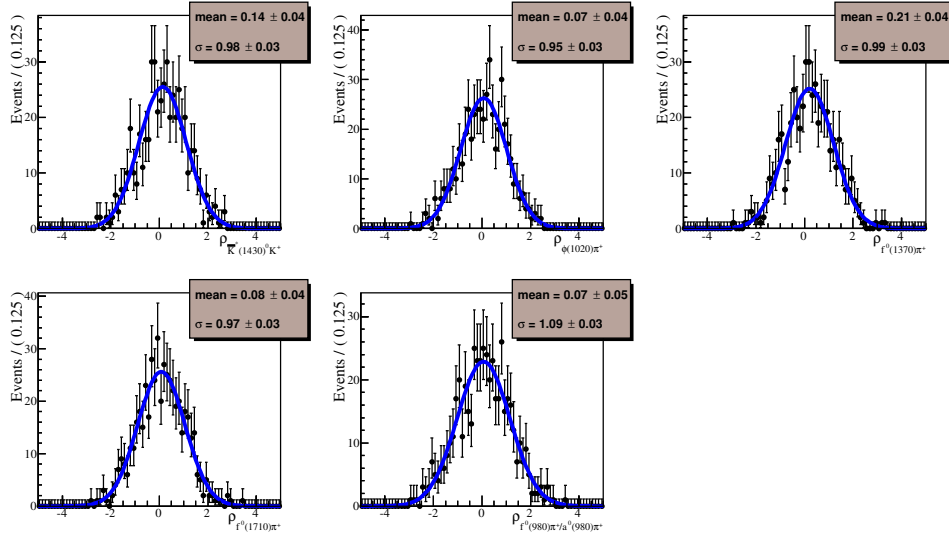


Figure 17: The pull distribution check results for magnitudes of the amplitudes in the nominal fit model.

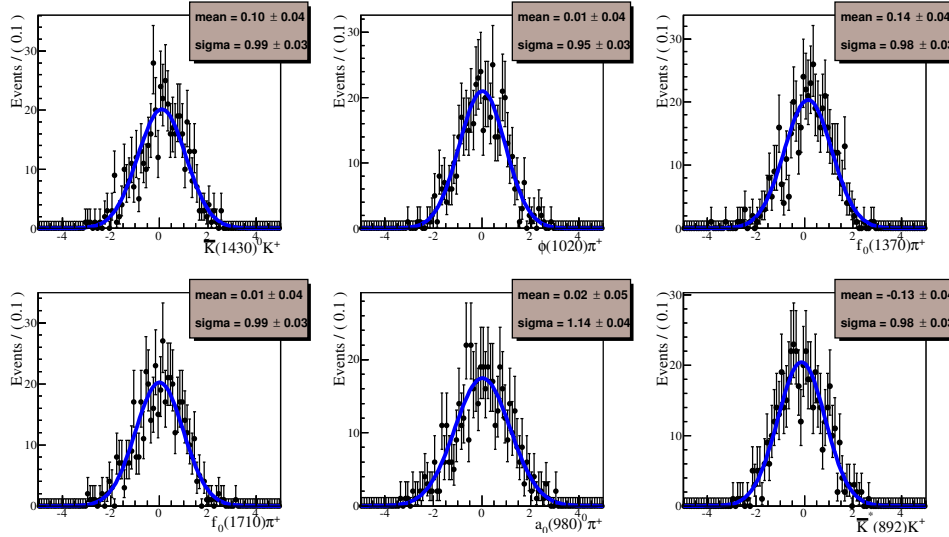


Figure 18: The pull distribution check results for fit fractions of the amplitudes in the nominal fit model.

Table 10: The DT efficiencies(ϵ_{DT}).

Tag mode	$\epsilon_{DT}(\%)$
$D_s^- \rightarrow K_S^0 K^-$	19.61 ± 0.14
$D_s^- \rightarrow K^+ K^- \pi^-$	18.26 ± 0.06
$D_s^- \rightarrow K^+ K^- \pi^- \pi^0$	4.68 ± 0.03
$D_s^- \rightarrow K_S^0 K^- \pi^+ \pi^-$	8.28 ± 0.11
$D_s^- \rightarrow K_S^0 K^+ \pi^- \pi^-$	9.52 ± 0.09
$D_s^- \rightarrow \pi^- \pi^- \pi^+$	23.55 ± 0.15
$D_s^- \rightarrow \pi^- \eta'_{\pi^+ \pi^-} \eta_{\gamma\gamma}$	8.28 ± 0.11
$D_s^- \rightarrow K^- \pi^+ \pi^-$	20.00 ± 0.19

6 Branching Fraction Measurements

6.1 Results of Branching Fraction

With the amplitude analysis results obtained from the fit to data, the double efficiencies without any kinematic fit requirement applied are determined and listed in Tab.10.

We divide the events into two categories:

- Cat. A: Tag D_s decays to tag modes except $D_s^- \rightarrow K_S^0 K^-$. The generic MC sample with the signal removed shows no peaking background around the fit range of $1.90 < M_{sig} < 2.03 GeV$. Thus, the double tag yield is determined by the fit to M_{sig} , which has shown in Fig.19(a). And the background is described with 2^{nd} -order Chebychev polynomial. The double tag yield is 3503 ± 64 .
- Cat. B: Tag D_s decays $K^+ K^- \pi^+$. As both of the two D_s mesons decay to our signal modes, we fit aM (the average mass of D_s at signal side and tag side), which is shown in Fig.19(b). Here, the background is described with 2^{nd} -order Chebychev polynomial. The double tag yield is 1629 ± 43 .

Then we can get the branching fraction $\mathcal{B}(D_s^+ \rightarrow K^+ K^- \pi^+) = (5.38 \pm 0.07)\%$ (only statistical uncertainty).

6.2 Systematic Uncertainties

The following sources are taken in account to calculate systematic uncertainties.

- Signal shape. The systematic uncertainty due to the signal shape is studied with the fit without the Gaussian function convoluted, the double tag yield shift is taken as the related effect.

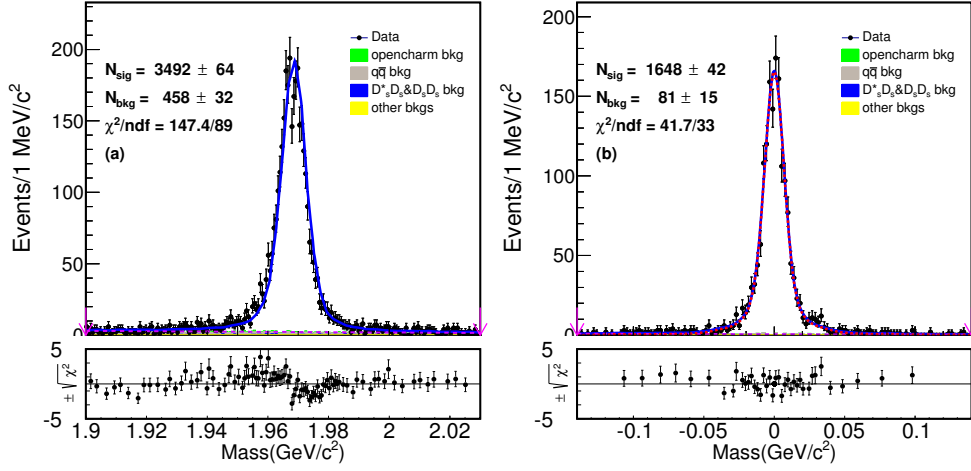


Figure 19: Fit of (a)Cat. A and (b)Cat. B. We fit M_{sig} and aM for Cat. A and Cat. B, respectively. The signal shapes are the corresponding simulated shapes convoluted with a Gaussian function and the background shapes are described with 2^{nd} -order Chebychev polynomial.

- Background shape and fit range. For background shape and the fit range, the MC shape is used to instead the 1^{st} -order Chebychev polynomial and the fit range of $[1.90, 2.03]GeV$ is changed to $[1.89, 2.04]GeV$. The largest branching fraction shift is taken as the related effect.
- Fit bias. The possible bias is estimated by the IO check with using the round 30-40 of generic MC.
- K^\pm and π^\pm Tracking/PID efficiency. Based on the works [11] and [12] by Xingyu Shan and Sanqiang Qu, etc, we find that it's enough to assign 1.1%, 0.4%, 1.1% and 0.2% as the systematic uncertainty for K^\pm PID, π^\pm PID, K^\pm tracking, π^\pm tracking efficiencies, respectively.
- MC statistics. The uncertainty of MC statistics is obtained by $\sqrt{\sum_i f_i \frac{\delta \epsilon_i}{\epsilon_i}}$, where f_i is the tag yield fraction and ϵ_i is the signal efficiency of tag mode i .

All of the systematic uncertainties mentioned above are summarized in Tab.11.

The branching fraction with systematic uncertainties is $\mathcal{B}(D_s^+ \rightarrow K^+ K^- \pi^+) = (5.38 \pm 0.07_{stat.} \pm 0.11_{sys.})\%$.

Table 11: Systematic uncertainties of branching fraction.

Source	Sys. Uncertainty
Signal shape	0.3
Background shape and fit range	1.1
Fit bias	0.2
K^\pm PID efficiency	1.1
π^\pm PID efficiency	0.4
K^\pm Tracking efficiency	1.1
π^\pm Tracking efficiency	0.2
MC statistics	0.2
total	2.0

Table 12: The result of this analysis.

Amplitude	Magnitude	Phase	Fit fractions(%)
$D_s^+ \rightarrow \bar{K}^*(892)^0 K^+$	1.0(fixed)	0.0(fixed)	$48.3 \pm 0.9 \pm 0.4$
$D_s^+ \rightarrow \phi(1020)\pi^+$	$1.09 \pm 0.02 \pm 0.01$	$6.22 \pm 0.07 \pm 0.04$	$40.5 \pm 0.7 \pm 0.9$
$D_s^+ \rightarrow f_0(980)\pi^+ / a_0(980)\pi^+$	$2.88 \pm 0.14 \pm 0.16$	$4.77 \pm 0.07 \pm 0.07$	$19.3 \pm 1.7 \pm 2.0$
$D_s^+ \rightarrow \bar{K}_0^*(1430)^0 K^+$	$1.26 \pm 0.14 \pm 0.15$	$2.91 \pm 0.20 \pm 0.23$	$3.0 \pm 0.6 \pm 0.5$
$D_s^+ \rightarrow f_0(1710)\pi^+$	$0.79 \pm 0.08 \pm 0.14$	$1.02 \pm 0.12 \pm 0.05$	$1.9 \pm 0.4 \pm 0.6$
$D_s^+ \rightarrow f_0(1370)\pi^+$	$0.58 \pm 0.08 \pm 0.08$	$0.59 \pm 0.17 \pm 0.45$	$1.2 \pm 0.4 \pm 0.2$

7 Summary

This analysis presents the amplitude analysis for the decay $D_s^+ \rightarrow K^+ K^- \pi^+$. The results are listed in Tab12.

We also measured the branching fraction and the value is $\mathcal{B}(D_s^+ \rightarrow K^+ K^- \pi^+) = (5.38 \pm 0.07_{stat.} \pm 0.11_{sys.})\%$.

This analysis will be used to do measurement of absolute hadronic branching fractions of D_s meson.

References

- [1] P.del Amo Sanchez *et al.* (BARBAR Collaboration), Phys. Rev. D**83**, 052001 (2011).
- [2] Andy Julin, Hajime Muramatsu and Ron Poling, BESIII DocDB 580-v1.
- [3] C. Patrignani *et al.* (Particle Data Group), Chin. Phys. C **40**,100001 (2016)
- [4] Sifan Zhang and Hailong Ma, BESIII DocDB 630-v35.
- [5] Yu Lu and Liaoyuan Dong, BESIII DocDB 416-v30.
- [6] B. S. Zou and D. V. Bugg, Eur. Phys. J. A**16**, 537(2003).
- [7] K. A. Olive *et al.* (Particle Data Group), Chin. Phys. C **40**, 100001 (2016)
- [8] M. Alblikim *et al.* (BESIII Collaboration), Phys. Lett. B**607** 243 (2005).
- [9] G. Bonvicini *et al.* (CLEO Collaboration), Phys. Rev. D**78**, 052001 (2001).
- [10] Yu Lu and Liaoyuan Dong, BESIII DocDB 613-v16.
- [11] <https://indico.ihep.ac.cn/event/8006/contribution/1/material/slides/0.pdf>
- [12] <https://indico.ihep.ac.cn/event/8023/contribution/1/material/slides/0.pdf>

¹ Appendices

1 A Subtract of the Secondary proton

2 A sizable of (anti-)proton candidates are produced from the electron/positron beam or particles in
 3 final states interacting with the MDC inner wall or residual gas inside beam-pipe, especially for proton.
 4 Here, we take the decay mode $\Lambda_c^+ \rightarrow p\eta(\gamma\gamma)$ as an example. Fig. ?? shows the compared V_T distributions
 5 of proton and anti-proton in different samples. In this analysis, we use the scaled inclusive MC to
 6 optimize the tight requirement with the $1/\sqrt{S+B}$ curve. Fig. 1 shows the efficiency distribution and
 7 $S/\sqrt{S+B}$ distribution with different V_T requirement. Where, S represents signal events, and B is scaled
 8 inclusive MC sample.